JCTC Journal of Chemical Theory and Computation

Article

pubs.acs.org/JCTC

Characterization of the Methane–Graphene Hydrophobic Interaction in Aqueous Solution from *Ab Initio* Simulations

C. Calero,*[,†,⊥] J. Martí,[†] E. Guàrdia,[†] and Marco Masia[‡,§,∥]

[†]Departament de Física i Enginyeria Nuclear, Universitat Politècnica de Catalunya-Barcelona Tech, B5-209 Campus Nord., 08034 Barcelona, Spain

[‡]Institut für Physikalische und Theoretische Chemie, Goethe Universität Frankfurt Max von Laue, Str. 7, D-60438 Frankfurt am Main, Germany

[§]Dipartimento di Chimica e Farmacia, Università degli Studi di Sassari, Via Vienna 2, 07100 Sassari, Italy

Supporting Information

ABSTRACT: In this article, the interaction between a methane molecule and a graphene plane in liquid water has been characterized employing DFT-based free energy Molecular Dynamics calculations. This system represents a good model to understand the generic interaction between a small hydrophobic solute (methane molecule) and an extense hydrophobic surface (graphene plane). The structural and dynamical properties of graphene and methane hydration water are analyzed and found to be closely related to the main features of the potential of mean force. The results could be used in coarse-grained models to take into account the effect of the hydrophobic interaction in realistic systems relevant to experiment.

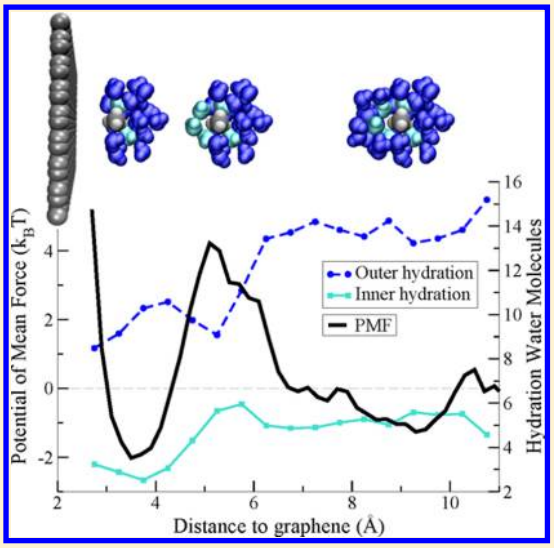

INTRODUCTION

A proper description of the interface of water with nonpolar materials at the atomic level is a fundamental problem, which has long been recognized to hold the key to the understanding of the hydrophobic effect,[1−5] which plays an important role in phenomena as diverse as protein folding, lipid aggregation, forces between hydrophobic surfaces in water, or chemical self-assembly of macroscopic objects.[6]

The impossibility for water molecules to create hydrogen bonds with nonpolar solutes has been identified to be the origin of the hydrophobic interaction.[4,5,7] Chandler and co-workers distinguish between two regimes, depending on the size of the hydrophobic unit. For small enough nonpolar particles, water molecules can reorganize around them without sacrificing hydrogen bonds. Such structural change has an entropic cost, which leads to low solubility of small nonpolar solutes in water. In contrast, next to a large nonpolar solute, the persistence of a hydrogen bond network is geometrically impossible. As a result, a thin layer next to the interface is formed where water molecules exhibit faster dynamics than in bulk. The existence of such layer can induce the appearance of strong interactions between large nonpolar solutes.[8−10] As a consequence of the existence of these two regimes, three kinds of two-body interactions can be distinguished between nonpolar solutes in water depending on their sizes (small–small, small–large, large–large).

In recent years, the improvement of existing experiments and the development of new surface sensitive experimental techniques[11] have provided a substantial amount of new information on the structure and dynamics of water at interfaces. In spite of such development, experimental data is often not conclusive, and hence, there is also a great need for theoretical analyses at the atomic scale. In that respect, the increase in computer power, the development of new algorithms, and the refinement of force fields that model the atomic interactions have permitted the study of extense realistic interfaces in contact with aqueous media employing classical computer simulations. A great amount of valuable insights on the features of water at interfaces has been obtained from classical molecular dynamics (MD) simulations.[12−15] However, the difficulty of accounting for the polarizability of atoms, the dependence of the analysis on the specific parametrization of the force field employed, and the impossibility of treating

Received: June 28, 2013
Published: September 17, 2013

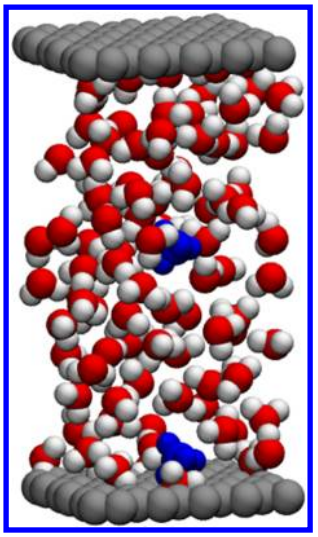

Figure 1. Snapshot of the simulation box for one of the restrained simulations performed. The gray spheres represent the carbon atoms of the graphene plane, the red and white spheres the oxigen and hydrogen atoms of the water molecule, and the blue atoms represent the atoms of the methane molecules. The distance between both methane molecules is greater than 1 nm.

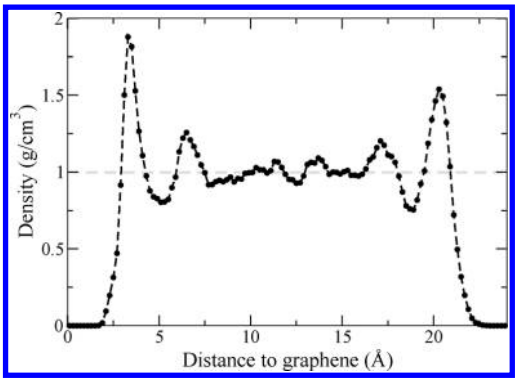

Figure 2. Water density profile obtained from the AIMD simulations. A large bulk region is present in the central part between the two graphene planes.

charge transfer or dissociation processes hinders the predictive power of such theoretical techniques. To circumvent those limitations, a considerable effort has been done in the description of aqueous systems with DFT-based *ab initio* molecular dynamics (AIMD) simulation techniques.[16,17] Recently, AIMD simulations studies of liquid water in contact with both small and large hydrophobic solutes have been reported.[18−21] In ref 18, the properties of water solvating a small nonpolar solute, a methane molecule, are investigated by Rossato et al. from first principles calculations. Li and co-workers studied in ref 19, the interaction between two methane molecules (small−small) dissolved in water using AIMD simulations and determined the properties of the solvation water as a function of the distance between methane molecules. In ref 20, Cicero et al. analyzed the structural and dynamical properties of D_2O confined in between graphene sheets (large−large), concluding that the perturbation on water properties induced by the extense hydrophobic surface is highly localized at the interface.

Our aim in this article is to establish a benchmark calculation for the potential of mean force of the interaction between a methane molecule and a graphene plane in water employing DFT-based first-principles calculations. With such a model system, we intend to quantitatively characterize the generic interaction between a small hydrophobic solute (methane molecule) and an extense hydrophobic surface (graphene plane).

METHODS

We applied the Umbrella Sampling technique[22] to accurately sample the relevant range of the potential of mean force, using artificial restraining harmonic potentials $1/2k(z - z_i)^2$ to confine the methane molecule within an interval centered around a given distance z_i from the graphene surface. In order to properly explore the whole range of interest, we performed a number of biased simulations, each one restraining the methane−graphene distance around successive values $\{z_i\}$. Once the restrained trajectories are obtained and the methane density from those restrained trajectories computed, we employed the Weighted Histrogram Analysis Method (WHAM)[23] to deconvolute the results and obtain the potential of mean force.

Given the inevitable presence of two interfaces (a vacuum−water interface in absence of any other layer) and based on the previous work by Cicero et al.[20] and on our own tests with classical simulations (see Supporting Information), we prepared for the AIMD simulations a symmetric system consisting of two 12.28 Å × 12.762 Å graphene sheets separated by 23.9 Å with 101 water molecules in between (see Figure 1). This system presents a wide enough water bulk region at the central part of the graphene sheets, which ensures a proper investigation of the whole range of the methane−graphene interaction in water (see Figure 2). The sampling statistics per simulation was doubled by considering two methane molecules (one per graphene layer) restrained at different distances z_i. In all simulations, the restraining potentials were centered at positions such that the two methane molecules were at least 1 nm apart. This distance is greater than the range of the methane−methane interaction in water,[19] which ensures that the presence of the methane molecules did not affect each other.

A series of seven independent ≈12-ps restrained AIMD simulations were performed, inspecting 14 different distances z_i in the range from 2 Å to 11 Å, in increments of 0.5 Å for $z < 6$ Å and of 1 Å for $z > 6$ Å. AIMD simulations were performed using the Quickstep algorithm as implemented in the cp2k package.[24] The PBE[25] functional was used for the electronic structure calculations, together with the DZVP (MOLOPT) Gaussian basis set[26] and Goedecker−Teter−Hutter[27−29] pseudopotentials. The density cutoff was set to 475 Ry to yield well converged calculations (see Supporting Information) at a reasonable computational cost. Grimme D3 dipersion parameters were used to correct for the well-known shortcomings of DFT methods in accounting for dispersion forces.[30] Equations of motion for the nuclei were integrated with the velocity Verlet algorithm using a time step of 0.5 fs. Quicker convergence of the wave function during dynamics was attained using the ASPC algorithm of Kolafa.[31] Periodic boundary conditions were applied along the three directions. A pre-equilibration of the system with 1 ns classical MD simulations was followed by a 2 ps equilibration at the DFT level. Thermal equilibrium in the canonical ensemble was reached using the CSVR thermostat[32] with a strong coupling. Production runs of ≈12 ps followed, where the canonical ensemble was sampled

dx.doi.org/10.1021/ct400554q | J. Chem. Theory Comput. 2013, 9, 5070−5075

using a weak coupling of the bath. The reference temperature was set to T_r = 298 K.

Restrained classical molecular dynamical simulations were performed to determine the appropriate size of the system and the parameters to be used in the *ab initio* calculations (see Supporting Information). In addition, we performed Adaptive Biasing Force (ABF) classical MD simulations[33,34] of an analogous larger system (with a 29.02 Å × 30.83 Å graphene sheet and 1615 water molecules), which will be used to compare with the PMF obtained via restrained *ab initio* MD simulations. We performed a total of 5 different MD-ABF runs of 1.5 ns each in order to obtain the potential of mean force of methane as a function of the distance to the graphene plane with 0.1 Å resolution. All classical MD simulations were performed using the 2.7 version of the NAMD simulation package running in parallel. The Newton equations of motion were solved with a time step of 2 fs and electrostatic interactions were updated with a 4 fs time step. All bonds between heavy atoms and hydrogen atoms were maintained rigid during all the simulation. The nonbonding Lennard-Jones interactions were cutoff at a distance of 1.2 nm employing a switching function starting at 1.0 nm. The particle mesh Ewald summation method was employed with a grid size of 1 Å. A constant temperature of T_r = 298 K was kept in all simulations using a Langevin thermostat with a relaxation constant of 1 ps^{-1}. In the classical MD simulations, water molecules are described by a modified TIP3P model following the standard specifications of the CHARMM22−27 force field. Both the graphene planes, prepared with the help of VMD,[35] and methane molecules are modeled employing the CHARMM22−27 force field parameters .[36]

RESULTS

In Figure 3, we show the main result of this work, namely the potential of mean force of the interaction of a methane

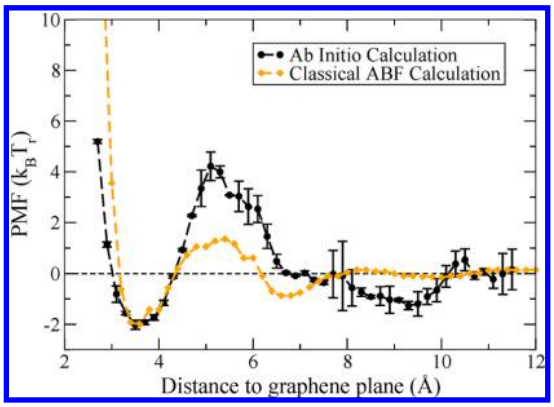

Figure 3. Potential of mean force of the methane−graphene interaction in water as a function of their mutual distance. Black circles: result obtained from restrained AIMD simulations. Orange diamonds: PMF calculated from classical ABF MD simulations.

molecule with a graphene plane immersed in water as a function of their mutual distance, using *ab initio* calculations. The dots represent the result obtained after deconvoluting all the restrained trajectories with the help of the WHAM technique. The error bars represent an estimate of the uncertainty of the results and were obtained by comparing the results obtained for the PMF from the first and second halves of the restrained trajectories. The PMF consists of a ∼ $4k_BT_r$ free energy barrier, which separates the bulk from an energetically favorable region (∼ $2k_BT_r$ deep) corresponding to the methane−graphene contact. Interestingly, in spite of the small size of the simulated system, our first-principles calculations are able to capture and quantify the effect of the water-mediated *hydrophobic* attraction between small and large nonpolar solutes. In the same graph, we also present the potential of mean force obtained from classical ABF-MD simulations (see Supporting Information for details.) Both results exhibit a qualitatively similar behavior, consisting of a free energy barrier that separates the bulk from an energetically favorable region next to the graphene plane. However, although the depth of the free energy minimum next to the graphene plane is almost identical, the height of the energy barrier separating that region from the bulk is significantly higher for the *ab initio* calculation.

As it is shown below, the appearance of the free energy barrier can be related to the work needed to release water molecules from the hydration layer of methane when it approaches the graphene plane. Inspection of the density profiles of water around methane from the classical and *ab initio* simulations performed reveals a considerably higher concentration of water in contact with methane in the *ab initio* description (see Supporting Information), which is an indication of an enhancement of water structure. Thus, the higher energy barrier obtained in the *ab initio* calculations is a consequence of the presence in that case of a more structured water layer hydrating methane.

To better understand the free energy profile we have analyzed several structural and dynamical properties of water hydrating methane and in contact with the graphene plane. We have computed such properties averaging over the generated trajectories, which amounts to ≈80 ps simulated time.

In Figure 2, the water density in the direction perpendicular to the graphene plane is represented. Note that it exhibits a high degree of symmetry along the direction perpendicular to the planes (it has not been artificially symmetrized), which indicates a proper equilibration of the system. As it is typical of a liquid in contact with a hard wall, density oscillations are observed at the interface, extending up to ≈1 nm, and evidencing a layering of water molecules. In agreement with recent classical[37−39] and *ab initio* calculations[20] of water in contact with hydrophobic surfaces, we observe a 2.5 Å thick exclusion region next to the graphene sheet followed by a pronounced maximum of the water density, almost doubling its bulk value. Next, there is a minimum followed by a clear second maximum and another minimum which rapidly decays to the bulk water density value.

The orientation of water molecules at the interface with the graphene plane has also been investigated. In Figure 4, we show several histograms for the orientation between the OH vector and the normal to the graphene plane for water molecules within 0.5 Å width layers centered at different distances from the surface. As it was found in previous studies of similar systems,[20,37] interfacial water exhibits strong preferential orientations. This is shown in Figure 4, in which a layering effect of water molecules in the vicinity of the graphene plane is evidenced. Indeed, while the OH bonds of interfacial water have an average orientation along the direction parallel to the surface (with $\cos\theta \approx 0$), the OH bonds of water molecules closest to the surface (at $z \approx 2.75$ Å) are preferentially oriented toward the bulk, whereas for the water layer centered at 3.75 Å the OH bond has a preferred orientation toward the graphene

dx.doi.org/10.1021/ct400554q | J. Chem. Theory Comput. 2013, 9, 5070−5075

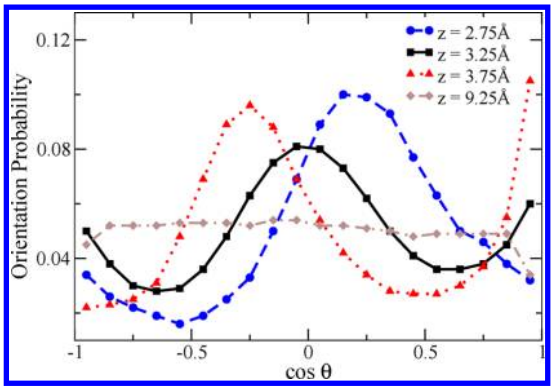

Figure 4. Histogram for the orientations of the OH vector of water molecules at the interface with the graphene plane. Each one of the curves corresponds to the orientation of a 0.5 Å width layer of water molecules centered at different distances from the graphene plane: 2.75 Å (blue dots), 3.25 Å (black squares), 3.75 Å (red triangles), and 9.25 Å (brown diamonds).

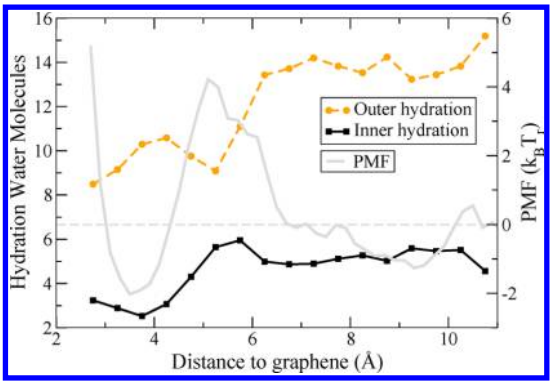

Figure 6. Number of water molecules at the outer (dashed orange line) and inner (solid black line) regions of the hydration shell as a function of the distance between the methane molecule and the graphene plane. Superimposed, we show the potential of mean force calculated from the analysis of *ab initio* molecular dynamics simulations (solid gray line).

surface. As shown in Figure 4, water molecules located far enough from the interface (at $z \approx 9.25$ Å, for example) are isotropically oriented.

In Figure 5, the average number of hydrogen bonds per water molecule are shown as a function of the distance to the graphene plane. We chose a geometric criterion to define hydrogen bonds in which the distance between the oxygen atoms of two hydrogen bonded molecules need to be smaller than 3.5 Å (first minimum in the O−O pair distribution function) and the angle O−H···O is smaller than 30°. We distinguish between hydrogen bond acceptors and donors and see that at the interface there is a depletion of H-bond acceptors and a certain increase of H-bond donors. This is a clear consequence of the layering phenomena in the orientation of water molecules at the graphene surface shown in Figure 4, in which the hydrogen atoms of the water molecules closest to the interface are oriented toward the bulk whereas the hydrogen atoms of subsequent water layers are oriented toward the surface.

We have studied the effect that hydration water has on the interaction between the methane molecule and the graphene layer. A water molecule is defined to be in the hydration shell of

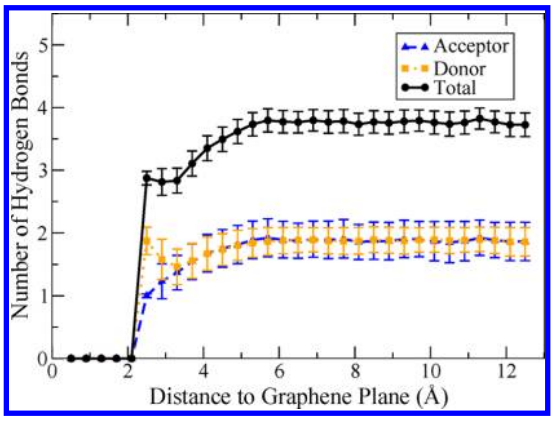

Figure 5. Average number of hydrogen bonds per water molecule as a function of the distance to the graphene plane. Triangle and square symbols represent the number of H-bond acceptor and donor per water molecule, respectively. Circular symbols represent the total number of hydrogen bonds per water molecule.

methane if the distance between its oxygen and the methane molecule is smaller than the location of the first minimum of the C−O pair correlation function (at 5.2 Å). The structure of hydration water around the methane molecule is determined by the competition between the weak interaction between water and methane and the strong water−water interaction. Among hydration water molecules, it is convenient to distinguish those which are in contact with the methane molecule (at the inner region of the hydration shell), defined here as the water molecules whose oxygen atoms are at a distance from the methane molecule smaller than the location of the first maximum of the C−O correlation function (at about 3.6 Å), and those which are at the outer region. As it has been theoretically predicted[4,5] and confirmed in classical and *ab initio*[18] simulation studies, the hydrogen-bond structure of water in contact with small hydrophobic solutes such as methane is enhanced, with HB average lifetimes longer than in bulk.[18]

In Figure 6, we represent the number of water molecules at the inner and outer regions of the hydration shell as a function of the distance between the methane molecule and the graphene plane. Superimposed on the same figure we show the potential of mean force calculated with *ab initio* simulations. The results reported in Figure 6 indicate that the appearance of the free energy barrier when the methane molecule approaches the graphene plane can be related to the release of water molecules from the methane's hydration shell. Indeed, the total number of water molecules in the hydration shell (inner + outer regions) decreases from a value of ≈19 in bulk to ≈14.5 when the methane molecule is located at the maximum of the free energy barrier. However, in such approaching process, only the water molecules in the outer region of the hydration shell are released. In that range of methane positions the number of water molecules in the inner region of the hydration shell even increases slightly, probably due to compression, and it is not until the methane molecule has overcome the free energy barrier that the water molecules in the inner region of the hydration shell are released, from a value of ≈5 in bulk to ≈2.5 water molecules when the methane molecule is at the stable free energy minimum. Thus, this decomposition suggests that the work needed to release water molecules from the outer region of the hydration shell of methane is responsible for the appearance of the free energy barrier in the PMF. Once some

dx.doi.org/10.1021/ct400554q | J. Chem. Theory Comput. 2013, 9, 5070−5075

of those outer molecules have been extracted, the release of half of the water molecules in the inner region of the hydration shell occurs spontaneously, lowering the free energy until the stable minimum at $z \approx 3.5$ Å. Such behavior is not exclusive of the *ab initio* description, but a similar relation between the energy barrier and the structure of the hydration shell of methane is found from the analysis of classical MD simulations (see Supporting Information). However, in our classical simulations, the hydration layer of methane contains less water molecules and it is less structured than in the *ab initio* calculations, inducing the appearance of a lower energy barrier.

Distinct structural patterns in the different regions of the system give rise to various dynamical behaviors. As a measure of water dynamics, we represent in Figure 7 the dipole rotational

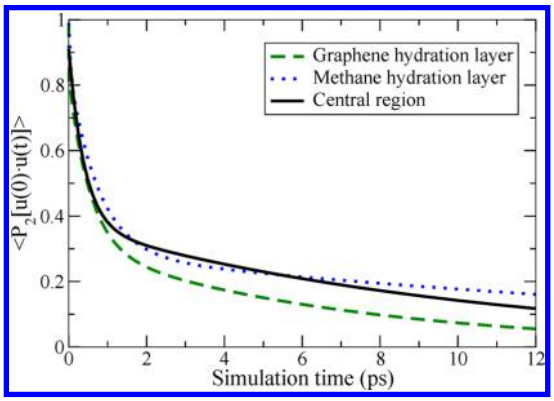

Figure 7. Rotational autocorrelation function $\langle P_2[\mathbf{u}(t)\cdot\mathbf{u}(0)]\rangle$ of water at the surface with the graphene planes (dashed green line), hydrating the methane molecule (dotted blue line), and at the central region between the graphene planes (solid black line).

autocorrelation function, $\langle P_2[\mathbf{u}(t)\cdot\mathbf{u}(0)]\rangle$ ($\mathbf{u}$ is the direction of the geometrical dipole and $P_2(x)$ is the second Legendre polynomial), calculated for water molecules at the interface with graphene (within the first minimum of the density profile), at the hydration layer of methane, and at the central region between graphene planes (water molecules further than 7 Å from the graphene planes). We have successfully fitted the relaxation of the autocorrelation function $\langle P_2[\mathbf{u}(t)\cdot\mathbf{u}(0)]\rangle$ with the help of biexponential functions $f_i(t)$, with i denoting the different regions, in order to compute their corresponding correlation times $\tau_i \equiv \int_0^\infty f_i(t)\mathrm{d}t$. The results, displayed in Figure 7 and in Table 1, show that the relaxation of the dipole rotational autocorrelation functions for those water molecules at the interface with the graphene plane is faster than for waters within the central region, whereas it is slower for those water molecules at the hydration layer of methane. These results are in accordance with previous results for confined water[20] and water hydrating small nonpolar solutes,[18] and agree with the theoretical approach to hydrophobicity introduced by Chandler and co-workers.[4,5] Indeed, our results on the water dynamics suggest that the structure of liquid water is enhanced for water molecules hydrating small hydrophobic solutes (i.e., methane molecules). This enhancement results in a reduction of the entropy of the system, as can be obtained from the analysis of the thermodynamics of tranfer of hydrocarbon chains to water.[40] In contrast, water molecules at the interface with graphene exhibit a faster reorientation than in bulk. This is due to the lower number of hydrogen bonds created at the interface (see Figure 5), a consequence of the impossibility to maintain the hydrogen bond network next to extense hydrophobic surfaces. A similar tendency has been reported in reference to the aqueous liquid−vapor interface, with rotational dynamics being faster at the interface than in bulk.[41]

Table 1. Correlation Times τ_i of the Dipole Rotation Autocorrelation Functions $\langle P_2[\mathbf{u}(t)\cdot\mathbf{u}(0)]\rangle$ for Water Molecules at the Interface with Graphene, at the Hydration Layer of Methane, and at the Central Region between Graphene Planes (see text)[a]

region	τ_i (ps)	water molecules considered
graphene hydration layer	2.4	172
central region	4.1	197
methane hydration layer	8.0	87

[a]The number of water molecules considered to compute the relaxation of the autocorrelation function (and its corresponding correlation time) for each region results from the accumulation over the seven 12 ps simulation runs performed.

CONCLUSIONS

In this article, we have studied the interaction of a small nonpolar solute (methane molecule) and an extense apolar plane (graphene sheet) in liquid water using DFT-based first-principles calculations. In spite of its relevance in a wide range of phenomena, such water-mediated *hydrophobic* interaction between small and large nonpolar solutes had not been studied in such detail before.

In order to characterize the methane−graphene interaction, we have calculated the potential of mean force as a function of their mutual distance with the help of restrained AIMD simulations. The PMF consists of a $4k_BT_r$ free energy barrier, which separates the bulk from an energetically favorable region ($2k_BT_r$ deep) corresponding to the methane−graphene contact. Thus, our first-principles calculations are able to capture and quantify the effect of the water-mediated *hydrophobic* attraction between small and large nonpolar solutes.

Our analysis of the hydration water surrounding methane as a function of its distance to the graphene plane suggests that the appearance of the free energy barrier is related to the work that needs to be done to release water molecules from the outer region of the hydration shell of methane. In approaching the graphene plane, some of the water molecules hydrating methane, which are structured around the methane molecule to maximize the number of hydrogen bonds and minimize the free energy,[5,40] need to be released in coming in contact with graphene and the hydration layer is partially dismantled. The impossibility to form a complete hydration layer and to create hydrogen bonds with the graphene plane has a free energy cost, which is responsible for the increase of the total free energy of the system. In further approaching the graphene sheet, the fluctuations of the structure of water molecules in the inner region of the hydration shell of methane allow a direct contact of the methane molecule with graphene, which is energetically favored. Indeed, some of the water molecules in the inner region of the hydration shell of methane can be released, which increases the total entropy of the system. In addition, the total surface exposed to water by nonpolar species is reduced and the volume where water can form hydrogen bonds increased. The minimum of the calculated potential of mean force, at $\approx -2k_BT_r$, quantifies such preference. This value is in accordance with experiment since, being the methane molecule at the interface between a nonpolar substance (graphene) and water,

it corresponds approximately to half the free energy of transfer of methane from water to oil, $\Delta G/2 \approx -1.7 k_B T_r$.[40,42]

We have also studied the dynamics of water molecules by monitoring the dipole rotational autocorrelation function at different regions of the system. Our results confirm that the structure of liquid water is enhanced in the hydration shell of methane with respect to bulk water. This enhancement results in a reduction of the entropy of the system, as can be obtained from the analysis of the thermodynamics of tranfer of hydrocarbon chains to water.[40] In contrast, water molecules at the interface with graphene exhibit a faster reorientation than in bulk, which is a consequence of the impossibility to maintain the hydrogen bond network next to extense hydrophobic surfaces.

■ ASSOCIATED CONTENT

Supporting Information

Details of the preliminary classical Molecular Dynamics simulations and of the choice of parameters for the *ab initio* calculations are provided. This information is available free of charge via the Internet at http://pubs.acs.org/.

■ AUTHOR INFORMATION

Corresponding Author

*E-mail: carles.calero@upc.edu.

Present Addresses

[‖]Department of Chemistry, Boston University, 590 Commonwealth Avenue, Boston, MA 02215, U.S.A.

[⊥]Center for Polymer Studies and Department of Physics, Boston University, 590 Commonwealth Avenue, Boston, MA 02215, U.S.A.

Notes

The authors declare no competing financial interest.

■ ACKNOWLEDGMENTS

The authors thankfully acknowledge the computer resources, technical expertise, and assistance provided by the Barcelona Supercomputing Center—Centro Nacional de Supercomputación for the projects QCM-2012-1-0013 and QCM-2012-2-0014. C.C., E.G., and J.M. gratefully acknowledge financial support from the *Direcció General de Recerca de la Generalitat de Catalunya* (Grant 2009-SGR-1003) and the Spanish MINECO for grant No. FIS2012-394-C02-01. C.C. is a UPC postdoctoral fellow. M.M. acknowledges the funding from the University of Sassari.

■ REFERENCES

(1) Stillinger, F. H. *J. Solution Chem.* **1973**, *2*, 141−158.
(2) Tanford, O. *The Hydrophobic Effect: Formation of Micelles and Biological Membranes*; Wiley and Sons: New York, 1980; pp 4−24.
(3) Israelachvili, J. *Intermolecular and Surface Forces*; Academic Press: London, 1992; pp 151−166.
(4) Lum, K.; Chandler, D.; D.Weeks, J. *J. Phys. Chem. B* **1999**, *103*, 4570−4577.
(5) Chandler, D. *Nature* **2005**, *437*, 640−647.
(6) Terfort, A.; Bowden, N.; Whitesides, G. *Nature* **1997**, *386*, 162−164.
(7) Lee, C.-Y.; McCammon, J. A.; Rossky, P. J. *J. Chem. Phys.* **1984**, *80*, 4448−4455.
(8) Pashley, R. M.; McGuiggan, P. M.; Ninham, B. W.; Evans, D. F. *Science* **1985**, *229*, 1088−1089.
(9) Christenson, H. K.; Claesson, P. M. *Science* **1988**, *239*, 390−392.
(10) Tsao, Y.-H.; Yang, S. X.; Evans, D. F.; Wennerstrom, H. *Langmuir* **1991**, *7*, 3154−3159.
(11) Verdaguer, A.; Sacha, G. M.; Bluhm, H.; Salmeron, M. *Chem. Rev.* **2006**, *106*, 1478−1510.
(12) Mamatkulov, S. I.; Khabibullaev, P. K.; Netz, R. *Langmuir* **2004**, *20*, 4756−4763.
(13) Huang, D. M.; Cottin-Bizonne, C.; Ybert, C.; Bocquet, L. *Langmuir* **2008**, *24*, 1442−1450.
(14) Schwierz, N.; Horinek, D.; Netz, R. *Langmuir* **2010**, *26*, 7370−7379.
(15) Godawat, R.; Jamadagni, S.; Garde, S. *Proc. Nat Acad. Sci. U.S.A.* **2009**, *106*, 15119−15124.
(16) Cavazzoni, C.; Chiarotti, G. L.; Scandolo, S.; Tosatti, E.; Bernasconi, M.; Parrinello, M. *Science* **1999**, *283*, 44−46.
(17) Schwegler, E.; Grossman, J.; Gygi, F.; Galli, G. *J. Chem. Phys.* **2004**, *121*, 5400−5409.
(18) Rossato, L.; Rossetto, F.; Silvestrelli, P. L. *J. Phys. Chem. B* **2012**, *116*, 4552−4560.
(19) Li, J.-L.; Car, R.; Tang, C.; Wingreen, N. S. *Proc. Natl. Acad. Sci. U.S.A.* **2007**, *104*, 2626−2630.
(20) Cicero, G.; Grossman, J.; Schwegler, E.; Gygi, F.; Galli, G. *J. Am. Chem. Soc.* **2008**, *130*, 1871−1878.
(21) Baer, M. D.; Mundy, C. J. *Phys. Chem. Lett.* **2011**, *2*, 1088−1093.
(22) Torrie, G. M.; Valleau, J. P. *Chem. Phys. Lett.* **1974**, *28*, 578−581.
(23) Kumar, S.; Bouzida, D.; Swendsen, R. H.; Kollman, P. A.; Rosenberg, J. M. *J. Comput. Chem.* **1992**, *13*, 1011−1021.
(24) VandeVondele, J.; Krack, M.; Mohamed, F.; Parrinello, M.; Chassaing, T.; Hutter, J. *Comput. Phys. Commun.* **2005**, *167*, 103−128.
(25) Perdew, J. P.; Burke, K.; Ernzerhof, M. *Phys. Rev. Lett.* **1996**, *77*, 3865−3868.
(26) VandeVondele, J.; Hutter, J. *J. Chem. Phys.* **2007**, *127*, 114105−114113.
(27) Goedecker, S.; Teter, M.; Hutter, J. *Phys. Rev. B* **1996**, *54*, 1703−1710.
(28) Hartwigsen, C.; Goedecker, S.; Hutter, J. *Phys. Rev. B* **1998**, *58*, 3641−3662.
(29) Krack, M. *Theor. Chem. Acc.* **2005**, *114*, 145−152.
(30) Grimme, S.; Antony, J.; Ehrlich, S.; Krieg, H. *J. Chem. Phys.* **2010**, *132*, 154104−154122.
(31) Kolafa, J. *J. Comput. Chem.* **2004**, *25*, 335−342.
(32) Bussi, G.; Donadio, D.; Parrinello, M. *J. Chem. Phys.* **2007**, *126*, 014101−014107.
(33) Darve, E.; Rodríguez-Gómez, D.; Pohorille, A. *J. Chem. Phys.* **2008**, *128*, 144120−144132.
(34) Hénin, J.; Fiorin, G.; Chipot, C.; Klein, M. L. *J. Chem. Theory Comput.* **2010**, *6*, 35−47.
(35) Humphrey, W.; Dalke, A.; Schulten, K. *J. Mol. Graphics* **1996**, *14*, 33−38.
(36) Phillips, J. C.; Braun, R.; Wang, W.; Gumbart, J.; Tajkhorshid, E.; Villa, E.; Chipot, C.; Skeel, R. D.; Kale, L.; Schulten, K. *J. Comput. Chem.* **2005**, *26*, 1781−1802.
(37) Gordillo, M.; Martí, J. *J. Phys.: Condens.Matter* **2010**, *22*, 284111−284118.
(38) Argyris, D.; Cole, D. R.; Striolo, A. *ACS Nano* **2010**, *4*, 2035−2042.
(39) Sala, J.; Guàrdia, E.; Martí, J. *Phys. Chem. Chem. Phys.* **2012**, *14*, 10799−10808.
(40) Widom, B.; Bhimalapuram, P.; Koga, K. *Phys. Chem. Chem. Phys.* **2003**, *5*, 3085−3093.
(41) Kuo, I.-F. W.; Mundy, C. J.; Eggimann, B. L.; McGrath, M. J.; Siepmann, J. I.; Chen, B.; Vieceli, J.; Tobias, D. J. *J. Phys. Chem. B* **2006**, *110*, 3738−3746.
(42) Southall, N. T.; Dill, K. A.; Haymet, A. D. J. *J. Phys. Chem. B* **2002**, *106*, 521−533.